

A Supramolecular Ice Growth Inhibitor

Ran Drori,^{*,†} Chao Li,[†] Chunhua Hu,[†] Paolo Raiteri,[‡] Andrew L. Rohl,[‡] Michael D. Ward,[†] and Bart Kahr^{*,†,§}

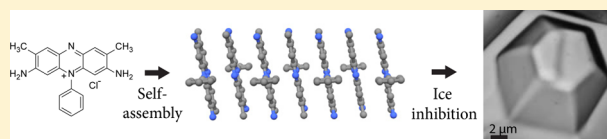
[†]Department of Chemistry and Molecular Design Institute, New York University, New York, New York 10003, United States

[‡]Curtin Institute for Computation and Department of Chemistry, Curtin University, Perth, Western Australia 6845, Australia

[§]Department of Advanced Science and Engineering (TWIns), Waseda University, Tokyo, Japan

Supporting Information

ABSTRACT: Safranin O, a synthetic dye, was found to inhibit growth of ice at millimolar concentrations with an activity comparable to that of highly evolved antifreeze glycoproteins. Safranin inhibits growth of ice crystals along the crystallographic *a*-axis, resulting in bipyramidal needles extended along the <0001> directions as well as and plane-specific thermal hysteresis (TH) activity. The interaction of safranin with ice is reversible, distinct from the previously reported behavior of antifreeze proteins. Spectroscopy and molecular dynamics indicate that safranin forms aggregates in aqueous solution at micromolar concentrations. Metadynamics simulations and aggregation theory suggested that as many as 30 safranin molecules were preorganized in stacks at the concentrations where ice growth inhibition was observed. The simulations and single-crystal X-ray structure of safranin revealed regularly spaced amino and methyl substituents in the aggregates, akin to the ice-binding site of antifreeze proteins. Collectively, these observations suggest an unusual link between supramolecular assemblies of small molecules and functional proteins.



INTRODUCTION

Life in polar climates depends on highly evolved antifreeze proteins and glycoproteins (AF(G)Ps)^{1–3} that irreversibly adsorb to ice,^{4,5} thereby inhibiting crystal growth. Some AFPs contain relatively rigid folded regions characterized by regularly spaced residues (e.g., threonines) that are purported to organize water molecules into motifs that are commensurate with the hexagonal ice crystal structure.^{6–8} Such noncolligative ice growth inhibitors induce a thermal hysteresis (TH), that is, a difference between the melting point and nonequilibrium freezing point of ice,^{9,10} a tell-tale signature of active binding at the ice interface. In addition to the survival of polar organisms, the inhibition of ice growth is essential for cryopreservation of food¹¹ and tissues,¹² as well as the synthesis of ice-templated materials.¹³ Synthetic compounds, however, exhibit only modest ice crystallization inhibition and do not cause substantial TH.^{14–22} Inexpensive and efficient ice growth inhibitors that mimic the effect of AF(G)Ps would be welcome.

Organic dyes are well-known to influence crystal growth and often become incorporated into specific facets of crystals.^{23,24} We considered whether dye molecules could affect the growth of ice crystals, particularly given their propensity to form aggregates in solution that could serve as mimics of AF(G)Ps through the periodic presentation of functional groups. The so-called lyotropic chromonic liquid crystal (LCLC) mesogens^{25–27} are illustrative in this respect owing to their ability to form supramolecular stacks consisting of a large number of regularly spaced molecules. We examined a library of 27 water-soluble dyes, some which had been reported to form LCLCs. Surprisingly, we discovered that only one compound from this library, safranin O chloride (S⁺Cl[−], Color Index number 50240, CAS number

477-73-6), a histochemical stain,²⁸ affects ice crystal growth. Optical spectroscopy, single-crystal X-ray analysis, aggregation theory, and metadynamics calculations implicate large aggregates of S⁺Cl[−] in ice growth inhibition (Figure 1).

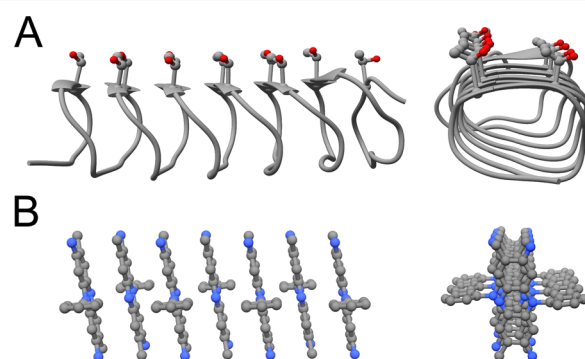


Figure 1. (A) Side and front views of *TmAFP*, an AFP from the mealworm *Tenebrio molitor*. (B) Side and front view of a stack of seven S⁺Cl[−] molecules, as observed in its single-crystal structure. Both *TmAFP* and the S⁺Cl[−] stacks are characterized by flat surfaces and periodic arrays thought to participate in binding at the ice interface.

EXPERIMENTAL SECTION

Dyes. A complete list of the dyes used in this study is included in Table S1. The dyes were tested for ice growth inhibition without further purification. Later, S⁺Cl[−] (Acros Organics, Fair Lawn, NJ), and

Received: August 8, 2016

Published: September 12, 2016

MV⁺Cl⁻ (methylene violet 3RAX, Color Index number 42535, CAS number 4569-86-2, Sigma Aldrich, St. Louis, MO) and P⁺Cl⁻ (phenosafranine chloride, Color Index number 50200, CAS number 81-93-6, Sigma Aldrich) purified by crystallization or by HPLC (see the Supporting Information for details). Ice growth inhibition of the pure compounds was comparable to that from as-obtained dye compounds.

Thermal Hysteresis Measurements and Crystal Morphology Characterization. We used a custom-designed cold stage with a temperature controller (Model 3040, Newport, Irvine, CA, USA) placed on an inverted microscope (DMIRE2, Leica Microsystems Inc., Buffalo Grove, IL), equipped with a sCMOS (Zyla 5.5, Andor, Belfast, UK) camera. We set a drop of immersion oil on a sapphire disc (1 in. diameter) upon the cold stage. A 0.5 μ L aliquot of an aqueous solution was injected inside the oil droplet, on top of which was placed a glass coverslip. This method prevented evaporation of water from the sample. The aqueous solution nucleated at ca. -20 $^{\circ}$ C, and the temperature was increased to melt the bulk ice, forming crystals at the desired size. A 980 nm IR laser (Wuhan Laserlands Laser Equipment Co., Ltd., China) melted unwanted ice. Once the desired crystal was obtained and the melting point was documented, the temperature was decreased at a rate of 0.075 $^{\circ}$ C/min until the crystal burst in the *a*-direction, reflecting a plane-specific TH activity.²⁰

Ice Growth Velocity Measurements. After obtaining crystals 20–30 μ m in width, a short pulse (1–2 s) of the IR laser melted the tip of the crystal, after which growth resumed, reforming the tip. Ice regrowth velocity was measured by video analysis.

Ice Recrystallization Inhibition. Concentrated aqueous sucrose solutions (45 wt %) best deposited separated ice crystals.²⁹ A 1 μ L aliquot of solution was placed on a sapphire disk, and a coverslip was placed on top of the droplet. To prevent evaporation, immersion oil was used to seal the cover glass. The sapphire–glass sandwich was set on a cold stage (Linkam LTS350, Linkam Scientific Instruments, Surrey, UK) which was mounted on an upright microscope (Axioskop 40, Carl Zeiss Microscopy, Jena, Germany), and the temperature was decreased to -45 $^{\circ}$ C at a rate of 40 $^{\circ}$ C/min. After the sample nucleated and frozen, the temperature was gradually increased to -6 $^{\circ}$ C and was then kept constant for the duration of the experiment. Images were collected every 2 min for 120 min.

Microfluidic Solution-Exchange Experiments. Polydimethylsiloxane (PDMS)-based microfluidic devices were fabricated following standard protocols (see Supporting Information for details). The device was placed on a sapphire disk (1 in. diameter), and immersion oil was applied between the layers. S⁺Cl⁻ solution was injected into the microfluidic channel, and the temperature was lowered until the liquid in the channel froze (typically at -20 $^{\circ}$ C). The temperature was then increased to melt the bulk ice. Unwanted ice was further melted with the IR laser described above. After a single ice crystal of \sim 30 μ m remained, the S⁺Cl⁻ solution was exchanged by injecting water into the channel.

Simulations. Details of metadynamics simulations are provided in the Supporting Information.

RESULTS

Ice crystal growth was examined by freezing a water droplet confined within oil at ca. -20 $^{\circ}$ C, increasing the temperature gradually until one crystal remained, and then reducing the temperature. At a supercooling of less than 0.5 $^{\circ}$ C, the ice crystals grew as {0001} plates,³⁰ reflecting higher growth rates along the *a*-axis relative to the *c*-axis (Figure 2). The crystals exhibited a cylindrical habit, indicating an isotropic surface energy for the crystal boundary parallel to the *c*-axis. The morphology of ice crystals grown in S⁺Cl⁻ solution (1.4–66 mM), however, was strikingly different. At low S⁺Cl⁻ concentrations (<3 mM), the crystals formed as hexagonal {0001} plates, with the large face oriented either parallel or perpendicular to the observation frame (Figure 2). At higher concentrations, however, we observed bipyramidal needles elongated on the *c*-axis (Figure 2). This signals interaction of S⁺Cl⁻ with specific faces on the ice surface that shape the crystal during growth. Some AF(G)Ps produce bipyramidal ice crystals with growth along the *c*-axis arrested

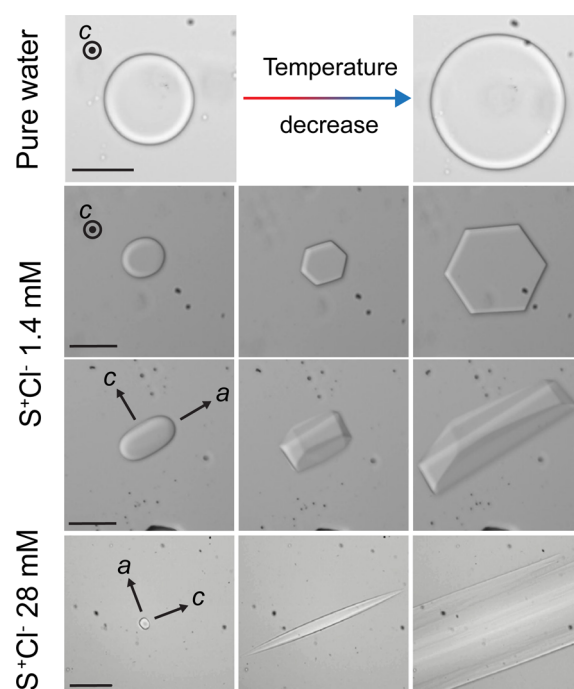


Figure 2. (top) Circular ice crystal at 0 $^{\circ}$ C, formed after melting bulk ice, grows by decreasing the temperature by 0.02 $^{\circ}$ C/min. (middle) Ice crystal growing in 1.4 mM S⁺Cl⁻ solutions with decreasing temperature at 0.36–0.12 $^{\circ}$ C/min. (bottom) Ice crystal growing in 28 mM with decreasing temperature at 0.075 $^{\circ}$ C/min. Temperature is decreasing left to right in all rows. The leftmost panels depict a crystal obtained by melting bulk ice previously formed between sapphire and glass surfaces. In the lower row, the melting point is -0.009 $^{\circ}$ C (left panel), and a burst in crystal growth was observed at -0.32 $^{\circ}$ C (rightmost panel). Scale bar = 20 μ m.

when the pyramidal planes converge.^{5,31,32} Ice growth in S⁺Cl⁻ solutions at concentrations >3 mM was distinct from that in the presence of AF(G)Ps, as growth along the *c*-axis did not stop while growth along the *a*-axis was negligible, resulting in long needles (Figure 2). As the temperature was lowered further, however, a sudden burst in crystal growth was observed along the *a*-axis (Movie S1). The temperature required for the crystal burst decreased with decreasing S⁺Cl⁻ concentration.

Ice growth inhibition by S⁺Cl⁻ was assessed quantitatively by measurement of the TH at various S⁺Cl⁻ concentrations. Therefore, the TH here is defined as a plane-specific TH, measured as the difference between the melting point and the temperature at which crystal growth bursts (the freezing point) along the *a*-axis. Plane-specific TH activity has been observed only once before (zirconium acetate) as we understand it.²⁰ Nonetheless, the plane-specific TH exhibited by S⁺Cl⁻ is compared with the TH values reported for AF(G)Ps in Figure 3A. Similar to AF(G)Ps, S⁺Cl⁻ did not significantly affect the melting point of ice crystals. Single crystals of ice (20–30 μ m in width) were grown by decreasing the temperature below the melting point at a fixed rate (0.075 $^{\circ}$ C/min) in solutions containing various concentrations of S⁺Cl⁻, up to its solubility limit (66 mM). The TH activity of S⁺Cl⁻ was not dependent on the rate of cooling (0.075–0.37 $^{\circ}$ C/min) or the time the crystal was exposed to S⁺Cl⁻ at constant temperature prior to cooling. This behavior is similar to AFPs that do not bind to the basal {0001} planes.⁹ As illustrated in Figure 3A, the TH activity for S⁺Cl⁻ (0.31 kDa) is less than that reported for TmAFP (9 kDa)^{9,10} and AFPIII (7 kDa)^{10,33} but similar to that of glycoprotein AFGP8 (2.6 kDa).³⁴

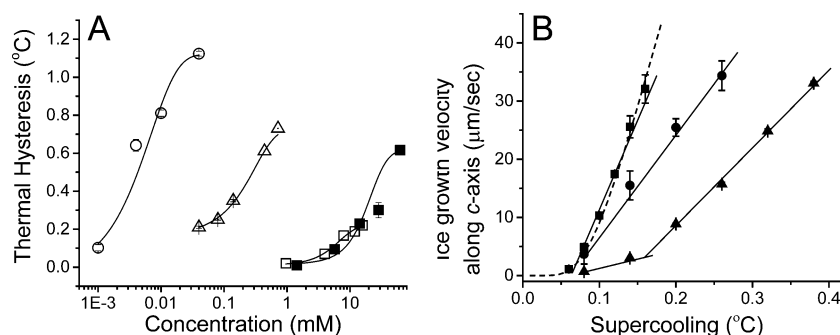


Figure 3. (A) Thermal hysteresis measured in the presence of various AF(G)Ps and S^+Cl^- , as measured from the inhibition of growth along the a -direction. The data is fitted to a sigmoidal form to replicate similar behavior reported for APFs: ^{35}O , $TmAFP$ -GFP (data from ref 9); Δ , AFPIII (data from ref 33); \blacksquare , S^+Cl^- ; \square , AFGP8 (data from ref 34). (B) Dependence of growth velocity along the c -axis on supercooling at different S^+Cl^- concentrations: \blacksquare , 14 mM; \bullet , 28 mM; \blacktriangle , 62 mM.

The growth velocity along the a -axis was negligible until the sudden burst of growth as the temperature was lowered, precluding measurement of growth velocity along this direction. The growth velocity along the c -axis was measurable, however, by locally heating the tip of a single crystal with an infrared laser and then tracking the advancement of the crystal tip along the c -axis. The c -axis growth velocity exhibited a so-called “dead zone” with respect to supercooling, after which the growth rate was linear. This behavior is consistent with step pinning³⁶ by S^+Cl^- , or its aggregates, due to adsorption at the growth interface (Figure 3B). The data clearly reveal that for a given supercooling, the growth velocity along the c -axis decreases with increasing S^+Cl^- concentration. Notably, the slopes at 14, 28, and 62 mM decreased with increasing S^+Cl^- concentration, which often is viewed as signaling a change in mechanism. This behavior may result from changes in the distribution of aggregate size and number of aggregates with increasing S^+Cl^- concentration, however, which precludes analysis based simply on the monomer concentration. Ostwald ripening of small ice crystals was suppressed at S^+Cl^- concentrations exceeding 4 mM, further supporting inhibition of crystallization by S^+Cl^- adsorption (Figure 4).

We examined the reversibility of S^+Cl^- adsorption for a single ice crystal (Figure 5A and Movie S2) formed in a microfluidic channel by melting a bulk ice crystal initially frozen at $-20^\circ C$ in a 14 mM S^+Cl^- solution. The solution containing the now well-defined hexagonal single crystal was then exchanged with neat water (Figure 5B), which was followed by an instantaneous crystal burst even though the temperature had not changed ($-0.302^\circ C$). Following the burst, the ice crystal grew as a round disc (Figure 5C) as a result of the reduction in the S^+Cl^- concentration in the surrounding medium due to exchange of the initial solution with neat water. This same experiment performed with the a - and c -axes of the ice crystal oriented parallel to the channel plane (Figure 5D–F) revealed growth along the a -axis when the S^+Cl^- was exchanged with neat water. These experiments demonstrate that S^+Cl^- inhibits ice growth but binds reversibly, in contrast to APFs^{4,5} that have a higher TH activity and bind irreversibly to the ice surface.

The crystal habits of ice in the presence of two congeners of S^+Cl^- were examined to elucidate the role of molecular structure on interaction with ice surfaces (Figure 6): methylene violet 3RAX (MV^+Cl^- , Color Index number 42535, CAS number 4569-86-2) and phenosafranine chloride (P^+Cl^- , Color Index number 50200, CAS number 81-93-6). Unlike S^+ , MV^+ carries one diethylamino group and lacks the arene methyl substituents, whereas P^+ differs

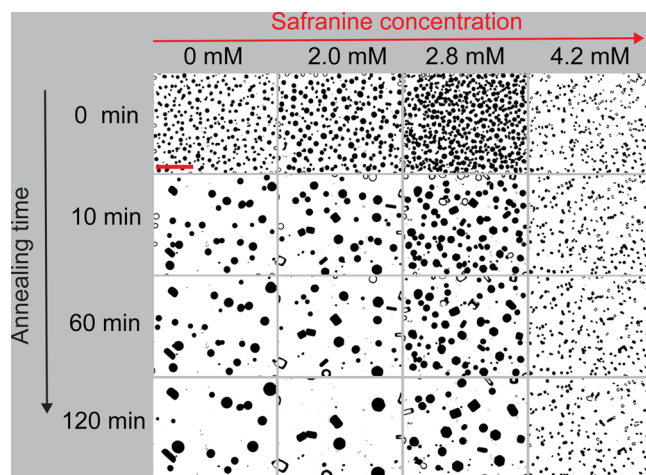


Figure 4. Evolution of ice crystals (black features) during 120 min at different S^+Cl^- concentrations following partial melting of bulk ice crystals. The number of crystals at 0 min was arbitrary and is not significant here. Hexagonal crystal shaping, implicating adsorption of S^+Cl^- to the surface, can be observed at 2.0 and 2.8 mM. Complete inhibition of Ostwald ripening was observed at 4.2 mM S^+Cl^- as the crystal size remained unchanged after 120 min. Red scale bar, upper left, is 100 μm .

from S^+ only by the absence of the methyl groups. Measurements could be performed only below the solubility limits for P^+Cl^- and MV^+Cl^- (~ 8 mM), but nonetheless, they permit a direct comparison with S^+Cl^- at these concentrations. Neither congener affected the morphology of ice crystals, nor did they inhibit growth.

The crystal structures of S^+Cl^- or the congeners have not been reported, despite the fact that azine dyes of this kind were among the earliest coal tar dyes.³⁷ The single crystal structures of MV^+Cl^- , P^+Cl^- , $S^+NO_3^-$, and S^+Cl^- (Figures S1–S4 and Tables S2 and S3) reveal stacks of centrosymmetric dimers with interplanar spacings of ~ 3.6 Å. The structures of MV^+Cl^- and P^+Cl^- revealed layers of water and chloride ions associated with the amino groups (Figures S1 and S2, respectively). These layers in S^+Cl^- , however, were disordered, precluding a determination of their organization. Nonetheless, the single-crystal structures suggest that aggregates of these dyes are capable of associating with structured water layers. Unlike S^+Cl^- , $S^+NO_3^-$ did not inhibit ice growth; no TH activity was observed up to the solubility limit (~ 5 mM), suggesting an important role for chloride ion. Indeed, addition of NaCl (final concentration = 0.05 M) to a solution containing $S^+NO_3^-$ restored the TH activity.

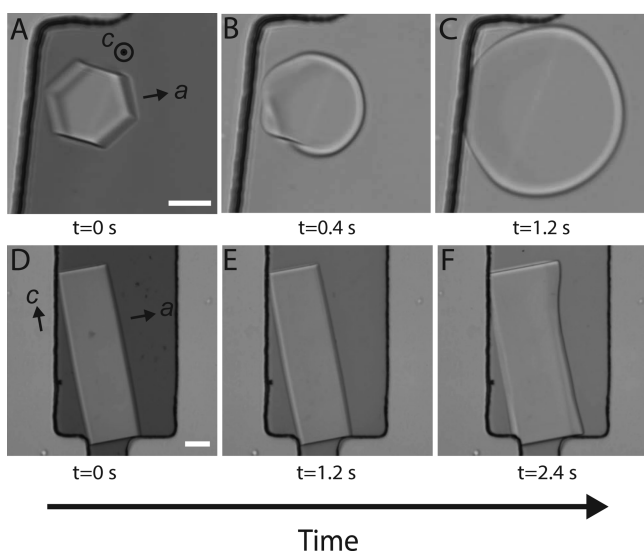


Figure 5. (A) Hexagonal ice crystal confined in a microfluidic channel. The channel prevented growth along the *c*-axis beyond the upper and lower surfaces of the channel. The crystal was formed by melting bulk ice in the presence of 14 mM S^+Cl^- . The S^+Cl^- dye is evident from the dark background due to light absorption. (B) The same crystal, after exchange of the S^+Cl^- solution with neat water, exhibits a round habit like that in the top panel of Figure 2. The transition between the hexagonal and rounded habit occurred in less than 0.4 s, the acquisition time of each frame. (C) Continued growth of the round ice crystal in the absence of S^+Cl^- . The temperature was constant throughout (-0.302 °C) at a supercooling of 0.047 °C. See Movie S2. (D–F) Similar experiment in which the initial ice crystal is oriented with the *a* and *c* axes in the plane of the channel. Exchange of 14 mM S^+Cl^- solution with neat water at -0.252 °C (supercooling of 0.04 °C) results in widening along the *a* axis. Scale bar = 20 μ m.

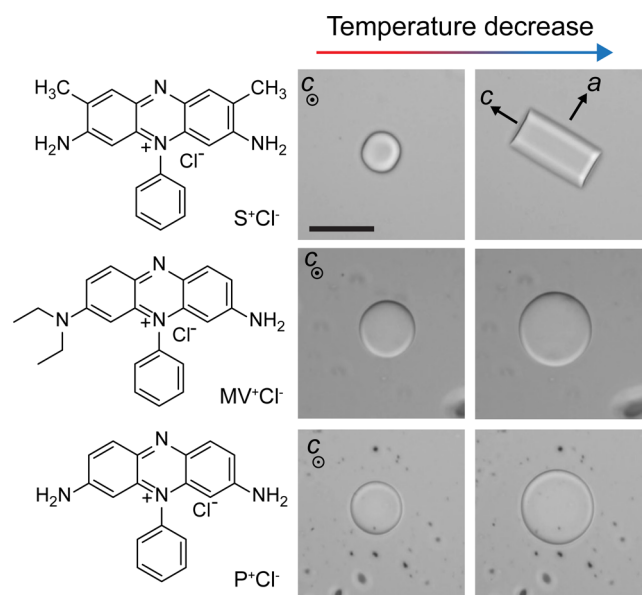


Figure 6. Growth habit of an ice crystal, formed by melting bulk ice in 8 mM solutions of S^+Cl^- , MV^+Cl^- , and P^+Cl^- . The discrimination of the ice interface for these dyes is clearly revealed by the change in habit. Scale bar = 20 μ m.

Metadynamics³⁸ was used to characterize the solution state of S^+Cl^- . Here, the sampling of configurational space was enhanced to retrieve a free energy hypersurface that connects all the stereoisomers of associated solute molecules. The free energy of

association of a S^+Cl^- dimer calculated with metadynamics exhibits a deep well for the associated state: the centric dimers evident in all crystal structures of this class of molecules. The metadynamics calculations predict scission energies of 20–24 kJ/mol for P^+Cl^- and 26–32 kJ/mol for S^+Cl^- (see Figures S5–S7). The scission energy calculated for S^+Cl^- is among the higher values of measured scission energies for similar dyes.³⁹

Aggregation theory⁴⁰ applied to associating lyotropic nematic mesogens,^{41,42} was used to estimate the average lengths of stacks from the scission energies and the molar volumes of the solutes according to eq 1, where N is the number of molecules in an aggregate, X_N is the volume fraction of an aggregate with N molecules, φ is the volume fraction obtained by dividing the solution concentration and molecular weight of the molecule by its density, and α is the scission free energy in units of kT . The average number of molecules in an aggregate, $\langle N \rangle$, can be calculated using eq 2. A comparison between P^+Cl^- and S^+Cl^- at a concentration of 8 mM reveals that $\langle N \rangle = 4$ and 15, respectively. For S^+Cl^- , over the concentration range of 1–66 mM, $\langle N \rangle = 6$ –30 supporting the existence of long aggregates of S^+Cl^- in solution. The metadynamics calculations predict a stacking motif that resembles that observed in the single-crystal structure. This aggregate structure presents alternating amine and methyl groups at an interface not unlike the hydroxyl and methyl groups of AFPs (Figure 1), suggesting a similar role for preorganized S^+Cl^- aggregates in ice crystal growth regulation.

$$X_N = N \left\langle \left(\frac{(1 + 2\varphi e^\alpha) - \sqrt{1 + 4\varphi e^\alpha}}{2\varphi e^{2\alpha}} \right)^N e^\alpha \right\rangle e^{-\alpha} \quad (1)$$

$$\langle N \rangle = \frac{\sum_{N=1}^{\infty} N(X_N/N)}{\sum_{N=1}^{\infty} (X_N/N)} \quad (2)$$

DISCUSSION

The observations above demonstrate that S^+Cl^- interacts specifically with the interfaces of ice crystals and inhibits growth. Within the thermal hysteresis gap, S^+Cl^- completely inhibits growth along the *a*-axis but not along the *c*-axis (Figure 2). The observation that ice growth along the *c*-axis was not completely inhibited and growth along the *a*-axis commenced after replacing S^+Cl^- solutions with neat water (Figure 5) argues that S^+Cl^- binds reversibly to ice surfaces, unlike AFPs.^{3,5,43} Reversible binding would seem to contradict the complete cessation of growth along the *a*-axis at S^+Cl^- concentrations exceeding 3 mM. This apparent contradiction likely reflects the supramolecular nature of the S^+Cl^- inhibitor, wherein growth inhibition is most effective at higher concentrations that favor bound aggregates. As the concentration of S^+Cl^- is reduced, aggregates can dissociate from the surface individually or as short segments, leaving smaller aggregates intact on the surface that continue to prevent growth. Only after reducing the S^+Cl^- concentration substantially would the aggregate coverage become sufficiently low to allow growth along the *a*-axis.

Inhibition by the S^+Cl^- aggregates is associated with adsorption at crystal growth sites, steps and kinks, on either the {0001} tips or the bipyramidal faces that define the flanks of the growing needle. The data in Figure 3B reveal a linear dependence of the step velocity which can be attributed to step pinning. Although the rate decreases with increasing S^+Cl^- concentrations as expected, the varied slopes of the linear curves suggest

contributions from kink blocking as well as step pinning or weak binding of the aggregates, which is consistent with the reversible binding discussed above.

Interpretation of this data is complicated by the increasing average aggregate size with increasing S^+Cl^- concentration and our inability to directly observe the micromorphology of the growth interfaces under these conditions. The needles grew along opposing directions from the initial ice crystal generated by melting bulk ice, with a constant central width defined by the seed. The observation of spirals generated by screw dislocations on the $\{0001\}$ faces of ice⁴⁴ suggests that growth along the c -axis can result from continual turning of spirals. This would be accompanied by an increase in the width of the basal plane behind the growth front as step train advances outward from the dislocation core(s) but can never exceed the boundary of the waist region. The decrease in growth along the c -axis with increasing S^+Cl^- concentration is consistent with $\{10\bar{1}0\}$ step pinning by aggregates on the $\{0001\}$ basal planes slowing the step advancement as well as the rate of spiral growth along the c -axis because the pinned sites afford step segments shorter than the critical length required for the spiral to turn. The bipyramidal planes of the ice needles could be characterized as vicinal, consisting of crystal planes parallel to the $[0001]$ zone axis (risers) and $\{0001\}$ planes (terrace). The aspect ratio of the needle indicates that the risers are longer than the terraces, although the increasing curvature of the needle closer to the tip is consistent with a reduction in the riser length relative to the terrace. The faster growth along the c -axis may reflect rapid advancement of the $\{0001\}$ steps along c and a negligible advancement along a . It is reasonable to suggest that the S^+Cl^- aggregates bind along the risers of the vicinal face, blocking advancement of $\{0001\}$ as was suggested for AFPs.³²

The plane-specific TH activity (along the a -axis) of S^+Cl^- solutions was comparable to that of AFGP8 (Figure 3A),³⁴ a natural ice growth inhibitor, but congeners of S^+ did not affect ice crystal morphology. It seems surprising that the absence of two methyl groups in P^+Cl^- would result in such a dramatic difference in ice growth and TH activity. This may be explained by differences in aggregation. As reported previously and confirmed in our laboratory, increasing concentrations of S^+Cl^- in water affords a blueshift in its absorption peak at micromolar concentrations, attributed to dimerization^{45,46} (Figure S8). This blueshift of the absorption peak has been observed for P^+Cl^- but only at twice the concentrations observed for S^+Cl^- .⁴⁶ This is consistent with the calculations above, which support the presence of S^+Cl^- stacks with $\langle N \rangle = 6-30$ over the concentration range at which S^+Cl^- inhibited ice growth (1–66 mM). In contrast, $\langle N \rangle = 4$ at the solubility limit of P^+Cl^- (8 mM). The stronger S^+Cl^- association is undoubtedly driven by increased dispersion interactions from methyl groups, and the exclusion of organized water around the solute.

The formation of preorganized stacked aggregates, implied here by experiment and computation, provides a reasonable explanation for ice growth inhibition by S^+Cl^- , which as a small molecule would otherwise not be expected to mimic the action of a protein. Recently, it was reported that the zirconium acetate complex that influences the morphology of ice crystals^{13,20} forms stacks in solution by using small-angle X-ray scattering (SAXS) and Raman spectroscopy.⁴⁷ Subtle effects, such as the absence of methyl groups in P^+Cl^- , reflect the sensitivity of molecular structure to aggregation and the corresponding activity for ice growth inhibition. This is reminiscent of the reduction in TH activity observed for mutations of otherwise active AFPs.⁴⁸

An ordered layer of water on the ice binding site of an AFP has been associated with binding of AFPs to ice.⁴⁹ An ordered water layer in the crystal structure of a bacterial AFP suggests that preorganization of icelike water is critical for inhibition.⁶ Ordered water molecules were found in crystal structures of other AFPs,^{8,50} and sum frequency generation indicated that icelike layers were formed on the ice-binding site of an AFP at ambient conditions in liquid water.⁵¹ MD simulations corroborated ordered water on protein interfaces involved in binding to ice surfaces.⁵² The observation of layers of water and Cl^- ions in S^+Cl^- (as well as P^+Cl^- and MV^+Cl^-), although disordered, is consistent with a similar ice-binding mode for S^+Cl^- aggregates.

In conclusion, a new small-molecule ice growth inhibitor has been discovered that is 10–100 times less massive than AF(G)Ps but exhibits inhibition characteristics similar to those reported for these proteins. Experimental evidence and computations implicate supramolecular aggregates that are characterized by a large scission energy and correspondingly large aggregate sizes. The preorganization achieved by aggregation reduces entropic barriers associated with the formation of ordered water layers and subsequent binding to the ice crystal interface. It is surprising that only 1 dye out of 27 exhibited ice growth inhibition, but the identification of the critical attributes underlying inhibition may provoke further discoveries of antifreeze molecules that emulate highly evolved proteins.

■ ASSOCIATED CONTENT

📄 Supporting Information

The Supporting Information is available free of charge on the ACS Publications website at DOI: 10.1021/jacs.6b08267.

X-ray crystal structures, metadynamics simulations, a complete list of tested dyes, and further experimental details (PDF)

Crystallographic information file for compounds $MV^+Cl^- \cdot H_2O$, $P^+Cl^- \cdot H_2O$, $S^+NO_3^- \cdot EtOH$ and $S^+Cl^- \cdot H_2O$ (CIF)
Movie S1, showing ice crystal growing at high S^+Cl^- concentration (28 mM) (AVI)

Movie S2, showing microfluidic solution-exchange experiment (AVI)

■ AUTHOR INFORMATION

Corresponding Authors

*droori.ran@gmail.com

*bart.kahr@nyu.edu

Notes

The authors declare no competing financial interest.

■ ACKNOWLEDGMENTS

This work was supported primarily by the NYU MRSEC Program of the National Science Foundation (NSF) under Award Number DMR-1420073 and by the NSF under Award Number DMR-1105000. The Bruker GADDS Microdiffractometer was acquired through the support by the NSF under Award Numbers CRIF/CHE-0840277 and the MRSEC Program under Award Number DMR-0820341. We acknowledge Chin Lin for his help with mass spectra measurements. We also thank Dr. Alexander Shtukenberg of New York University for helpful discussions and Dr. Yu-Sheng Chen at the ChemMatCARS Sector 15 of the Advanced Photon Source (APS), which is principally supported by the NSF (grant number CHE-1346572). Use of the APS, an Office of Science User Facility operated for the U.S. Department of Energy (DOE) Office of Science by Argonne

National Laboratory, was supported by the U.S. DOE under Contract Number DE-AC02-06CH11357. Funding was also provided by the Australian Research Council (grants FT130100463 and DP140101776). This work was supported by computational resources provided by the Pawsey Centre.

REFERENCES

- (1) Devries, A. L. *Science* **1971**, *172*, 1152.
- (2) Davies, P. L. *Trends Biochem. Sci.* **2014**, *39*, 548.
- (3) Duman, J. G. *J. Exp. Biol.* **2015**, *218*, 1846.
- (4) Celik, Y.; Drori, R.; Pertaya-Braun, N.; Altan, A.; Barton, T.; Bar-Dolev, M.; Groisman, A.; Davies, P. L.; Braslavsky, I. *Proc. Natl. Acad. Sci. U. S. A.* **2013**, *110*, 1309.
- (5) Drori, R.; Davies, P. L.; Braslavsky, I. *Langmuir* **2015**, *31*, 5805.
- (6) Garnham, C. P.; Campbell, R. L.; Davies, P. L. *Proc. Natl. Acad. Sci. U. S. A.* **2011**, *108*, 7363.
- (7) Davies, P. L.; Graether, S. P.; Kuiper, M. J.; Gagne, S. M.; Walker, V. K.; Jia, Z. C.; Sykes, B. D. *Nature* **2000**, *406*, 325.
- (8) Sun, T. J.; Lin, F. H.; Campbell, R. L.; Allingham, J. S.; Davies, P. L. *Science* **2014**, *343*, 795.
- (9) Drori, R.; Celik, Y.; Davies, P. L.; Braslavsky, I. *J. R. Soc., Interface* **2014**, *11*, 20140526.
- (10) Scotter, A. J.; Marshall, C. B.; Graham, L. A.; Gilbert, J. A.; Garnham, C. P.; Davies, P. L. *Cryobiology* **2006**, *53*, 229.
- (11) Kiani, H.; Sun, D.-W. *Trends Food Sci. Technol.* **2011**, *22*, 407.
- (12) Lewis, J. K.; Bischof, J. C.; Braslavsky, I.; Brockbank, K. G.; Fahy, G. M.; Fuller, B. J.; Rabin, Y.; Tocchio, A.; Woods, E. J.; Wowk, B. G.; Acker, J. P.; Giwa, S. *Cryobiology* **2016**, *72*, 169.
- (13) Deville, S.; Viazzi, C.; Leloup, J.; Lasalle, A.; Guizard, C.; Maire, E.; Adrien, J.; Gremillard, L. *PLoS One* **2011**, *6*, e26474.
- (14) Capicciotti, C. J.; Poisson, J. S.; Boddy, C. N.; Ben, R. N. *Cryobiology* **2015**, *70*, 79.
- (15) Congdon, T.; Notman, R.; Gibson, M. I. *Biomacromolecules* **2013**, *14*, 1578.
- (16) Gibson, M. I. *Polym. Chem.* **2010**, *1*, 1141.
- (17) Harding, M. M.; Anderberg, P. I.; Haymet, A. D. J. *Eur. J. Biochem.* **2003**, *270*, 1381.
- (18) Huang, M. L.; Ehre, D.; Jiang, Q.; Hu, C. H.; Kirshenbaum, K.; Ward, M. D. *Proc. Natl. Acad. Sci. U. S. A.* **2012**, *109*, 19922.
- (19) Wilkinson, B. L.; Stone, R. S.; Capicciotti, C. J.; Thaysen-Andersen, M.; Matthews, J. M.; Packer, N. H.; Ben, R. N.; Payne, R. J. *Angew. Chem., Int. Ed.* **2012**, *51*, 3606.
- (20) Mizrahy, O.; Bar-Dolev, M.; Guy, S.; Braslavsky, I. *PLoS One* **2013**, *8*, e59540.
- (21) Vorontsov, D. A.; Sazaki, G.; Hyon, S. H.; Matsumura, K.; Furukawa, Y. *J. Phys. Chem. B* **2014**, *118*, 10240.
- (22) Budke, C.; Koop, T. *ChemPhysChem* **2006**, *7*, 2601.
- (23) Buckley, H. E. Z. *Kristallogr.* **1930**, *73*, 443.
- (24) Kahr, B.; Gurney, R. W. *Chem. Rev.* **2001**, *101*, 893.
- (25) Collings, P. J.; Dickinson, A. J.; Smith, E. C. *Liq. Cryst.* **2010**, *37*, 701.
- (26) Lydon, J. *Curr. Opin. Colloid Interface Sci.* **2004**, *8*, 480.
- (27) Tam-Chang, S.-W.; Huang, L. *Chem. Commun.* **2008**, 1957.
- (28) Kiviranta, I.; Jurvelin, J.; Saamanen, A. M.; Helminen, H. J. *Histochemistry* **1985**, *82*, 249.
- (29) Budke, C.; Heggemann, C.; Koch, M.; Sewald, N.; Koop, T. *J. Phys. Chem. B* **2009**, *113*, 2865.
- (30) Hobbs, P. V. *Ice Physics*; Clarendon Press: Oxford, U.K., 1974.
- (31) Bar-Dolev, M.; Celik, Y.; Wettlaufer, J. S.; Davies, P. L.; Braslavsky, I. *J. R. Soc., Interface* **2012**, *9*, 3249.
- (32) Knight, C. A.; Cheng, C. C.; Devries, A. L. *Biophys. J.* **1991**, *59*, 409.
- (33) Stevens, C. A.; Drori, R.; Zalis, S.; Braslavsky, I.; Davies, P. L. *Bioconjugate Chem.* **2015**, *26*, 1908.
- (34) Tachibana, Y.; Fletcher, G. L.; Fujitani, N.; Tsuda, S.; Monde, K.; Nishimura, S. I. *Angew. Chem., Int. Ed.* **2004**, *43*, 856.
- (35) Marshall, C. B.; Chakrabarty, A.; Davies, P. L. *J. Biol. Chem.* **2005**, *280*, 17920.
- (36) Cabrera, N.; Vermilyea, D. A. *Growth and perfection of crystals*; Chapman and Hall: London, 1958.
- (37) Perkin, W. H. *J. Chem. Soc., Trans.* **1879**, *35*, 717.
- (38) Barducci, A.; Bussi, G.; Parrinello, M. *Phys. Rev. Lett.* **2008**, *100*, 020603.
- (39) Dickinson, A. J.; LaRacune, N. D.; McKitterick, C. B.; Collings, P. J. *Mol. Cryst. Liq. Cryst.* **2009**, *509*, 751.
- (40) Israelachvili, J. N. *Intermolecular and Surface Forces*, 3rd ed.; Academic Press: San Diego, CA, 2011.
- (41) Horowitz, V. R.; Janowitz, L. A.; Modic, A. L.; Heiney, P. A.; Collings, P. J. *Phys. Rev. E* **2005**, *72*, 041710.
- (42) McKitterick, C. B.; Erb-Satullo, N. L.; LaRacune, N. D.; Dickinson, A. J.; Collings, P. J. *J. Phys. Chem. B* **2010**, *114*, 1888.
- (43) Raymond, J. A.; Devries, A. L. *Proc. Natl. Acad. Sci. U. S. A.* **1977**, *74*, 2589.
- (44) Sazaki, G.; Asakawa, H.; Nagashima, K.; Nakatsubo, S.; Furukawa, Y. *Cryst. Growth Des.* **2014**, *14*, 2133.
- (45) Niazi, A.; Yazdanipour, A.; Ghasemi, J.; Kubista, M. *Spectrochim. Acta, Part A* **2006**, *65*, 73.
- (46) Sarkar, D.; Das, P.; Girigoswami, A.; Chattopadhyay, N. *J. Phys. Chem. A* **2008**, *112*, 9684.
- (47) Gossard, A.; Toquer, G.; Grandjean, S.; Grandjean, A. *J. Sol-Gel Sci. Technol.* **2014**, *71*, 571.
- (48) Bar, M.; Celik, Y.; Fass, D.; Braslavsky, I. *Cryst. Growth Des.* **2008**, *8*, 2954.
- (49) Nutt, D. R.; Smith, J. C. *J. Am. Chem. Soc.* **2008**, *130*, 13066.
- (50) Hakim, A.; Nguyen, J. B.; Basu, K.; Zhu, D. F.; Thakral, D.; Davies, P. L.; Isaacs, F. J.; Modis, Y.; Meng, W. *J. Biol. Chem.* **2013**, *288*, 12295.
- (51) Meister, K.; Strazdaite, S.; DeVries, A. L.; Lotze, S.; Olijve, L. L.; Voets, I. K.; Bakker, H. J. *Proc. Natl. Acad. Sci. U. S. A.* **2014**, *111*, 17732.
- (52) Kuiper, M. J.; Morton, C. J.; Abraham, S. E.; Gray-Weale, A. *eLife* **2015**, *4*, e05142.